



OPEN

SUBJECT AREAS:

FIBRE OPTICS AND
OPTICAL
COMMUNICATIONS

OPTICS AND PHOTONICS

Received
15 July 2013

Accepted
6 January 2014

Published
24 January 2014

Correspondence and
requests for materials
should be addressed to
J.W. (jwang@hust.
edu.cn)

A Compact Trench-Assisted Multi-Orbital-Angular-Momentum Multi-Ring Fiber for Ultrahigh-Density Space-Division Multiplexing (19 Rings \times 22 Modes)

Shuhui Li & Jian Wang

Wuhan National Laboratory for Optoelectronics, School of Optical and Electronic Information, Huazhong University of Science and Technology, Wuhan 430074, Hubei, China.

We present a compact (130 μm cladding diameter) trench-assisted multi-orbital-angular-momentum (OAM) multi-ring fiber with 19 rings each supporting 22 modes with 18 OAM ones. Using the high-contrast-index ring and trench designs, the trench-assisted multi-OAM multi-ring fiber (TA-MOMRF) features both low-level inter-mode crosstalk and inter-ring crosstalk within a wide wavelength range (1520 to 1630 nm), which can potentially enable Pbit/s total transmission capacity and hundreds bit/s/Hz spectral efficiency in a single TA-MOMRF. Moreover, the effective refractive index difference of even and odd fiber eigenmodes induced by the ellipticity of ring and fiber bending and their impacts on the purity of OAM mode and mode coupling/crosstalk are analyzed. It is found that high-order OAM modes show preferable tolerance to the ring ellipticity and fiber bending. The designed fiber offers favorable tolerance to both small ellipticity of ring (<-22 dB crosstalk under an ellipticity of 0.5%) and small bend radius (<-20 dB crosstalk under a bend radius of 2 cm).

Orbital angular momentum (OAM) beams characterized by a helical phase front of $\exp(il\phi)$ ¹, where l is the topological charge number, have been widely used in microscopy², particle trapping³, and photon entanglement⁴. Recently, using OAM beams as carriers in a communication system has gained much interest due to intrinsic spatial orthogonality of OAM modes with different topological charge numbers. OAM mode multiplexing has been realized in both free space and fiber communication systems^{5–8}. It is expected that space-division multiplexing (SDM) using OAM modes may offer an alternative to address the coming capacity crunch.

Most of previous reports of OAM mode multiplexing in a fiber adopt a single high-contrast-index ring-core structure^{7–10}. Such structure can reduce the inter-mode crosstalk and stably support multiple OAM modes. Although two or more OAM modes have been explored in this kind of fiber, more comprehensive analyses are required to clearly show how many modes can be well supported with low-level inter-mode crosstalk for an optimized design. In addition, one would also expect to see its compatibility with existing SDM techniques and fiber designs. In view of well-known SDM techniques using multi-core fiber (MCF) and few-mode fiber (FMF)^{11,12}, especially more recent works of few-mode multi-core fiber¹³, a laudable goal would be to combine OAM mode multiplexing and multi-core-like structure for high-capacity OAM communications^{14,15}, where both inter-mode crosstalk and inter-ring crosstalk and their suppression should be considered.

In this paper, we present an improved compact design of trench-assisted multi-OAM multi-ring fiber (TA-MOMRF) for ultrahigh-density SDM. The designed TA-MOMRF has 19 rings with each ring supporting 22 modes (18 OAM ones), i.e. 418 channels in total. The large difference of effective refractive index of fiber eigenmodes ($>10^{-4}$) in each ring enables low inter-mode crosstalk. The high-contrast-index ring and trench design ensure pretty low-level inter-ring crosstalk and give a compact structure. Wide-range operations covering the whole C and L bands are also available, which are compatible with well-established wavelength-division multiplexing (WDM) technique. The tolerance to birefringence induced by practical ellipticity of ring and fiber bending is studied.

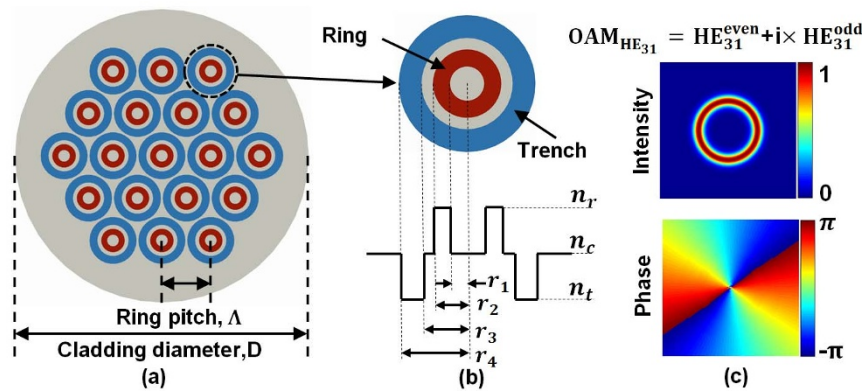


Figure 1 | (a) Cross-section of a 19-ring trench-assisted multi-OAM multi-ring fiber (TA-MOMRF). (b) Index profile of a single ring. (c) Intensity and phase distributions of HE_{31} related OAM mode in a single ring.

Results

Design of trench-assisted multi-OAM multi-ring fiber (TA-MOMRF). Figure 1(a) shows a schematic cross-section of the designed 19-ring TA-MOMRF. The ring pitch Λ and cladding diameter are 25 and 130 μm , respectively. Compared to previously reported 19-core fiber with the core pitch and cladding diameter of 35 and 200 μm ¹⁶, our structure is more compact. Trench-assisted high-contrast-index ring is adopted to support multiple OAM modes in each ring and greatly reduce the inter-ring crosstalk among 19 rings. The index profile of a single ring is illustrated in Fig. 1(b). The glasses used in the TA-MOMRF are (i) ring: Schott SF4 with $n_r = 1.72$, (ii) trench: Schott LLF1 with $n_t = 1.5$, (iii) cladding: Schott SF2 with $n_c = 1.62$ (at 1550 nm). Those materials of high-contrast-index structure have been utilized in previous fiber design for generating OAM modes^{9,10}. In addition, practical fabrication of special fiber using similar type of materials has also been reported^{17,18}. In the designed TA-MOMRF, the inner (r_1) and outer (r_2) radius of a single ring are 3 and 4 μm , respectively. The trench has an inner radius r_3 of 6 μm and an outer radius r_4 of 11 μm . As an example, the calculated intensity and phase distributions of HE_{31} related OAM mode in a single ring are depicted in Fig. 1(c).

Mode properties of the designed TA-MOMRF. Table 1 presents calculated effective refractive index (n_{eff}) of 12 different order fiber eigenmodes at 1550 nm supported by a single ring. Owing to the high-contrast-index ring structure design, the maximum difference of n_{eff} can be as high as 0.01335 between EH_{31} and EH_{41} modes, and even the minimum difference of n_{eff} can reach 0.00013 between EH_{41} and HE_{61} modes. Large difference of n_{eff} benefits efficient suppression of inter-mode crosstalk.

In fact, there are 22 fiber eigenmodes since each HE_{m1} or EH_{n1} mode also contains even and odd modes. One can obtain OAM modes by combine even and odd modes of HE_{m1} or EH_{n1} with a $\pm\pi/2$ phase shift¹⁹, i.e. $OAM_{HE_{m1}} = HE_{m1}^{\text{even}} \pm i \times HE_{m1}^{\text{odd}}$, $OAM_{EH_{n1}} = EH_{n1}^{\text{even}} \pm i \times EH_{n1}^{\text{odd}}$. The topological charge number of $OAM_{HE_{m1}}$ and $OAM_{EH_{n1}}$ is $\pm(m-1)$ and $\pm(n+1)$, respectively. As an example of the phase distribution of $OAM_{HE_{31}}$ shown in Fig. 1(c), the azimuthal phase variation is 4π corresponding to a topological charge number of 2. Hence, one can get 18 nonzero topological charge number

OAM modes. Considering the fundamental mode HE_{11} (x and y polarization), TE_{01} and TM_{01} modes, 22 modes (18 OAM ones) in total are supported with low-level inter-mode crosstalk in a single ring.

Inter-ring crosstalk of the designed TA-MOMRF. In addition to inter-mode crosstalk, another important parameter is inter-ring crosstalk in the designed TA-MOMRF. Similar to a multi-core fiber, the number of rings in the TA-MOMRF is limited by the ring pitch under a fixed cladding diameter. Small ring pitch gives more rings but leads to a large crosstalk between neighboring rings. To suppress the inter-ring crosstalk and increase the number of rings, trench design is employed.

In order to determine the ring pitch necessary for achieving negligible crosstalk, we employ coupled-power method to assess the crosstalk between two adjacent rings. The normalized power transfer between two identical rings is given by $\sin^2[\pi z/(2L_c)]$ with L_c being the coupling length and z being the propagation length²⁰. The coupled-mode theory method which has the ability to accurately evaluate ultralong coupling length ($\sim 10^{10}$ m)²¹ has been used to calculate L_c .

Figure 2 shows L_c of different OAM modes in adjacent rings as a function of Λ . It is found that L_c increases with Λ , which is easy to understand that large separation between adjacent rings can reduce mode overlap and power transfer between adjacent rings, resulting in a long L_c . One may note the oscillation in Fig. 2, which can be explained with the fact that the adopted coupled-mode theory features a calculation precision of $\sim 10^{10}$ m. However 10^{10} m coupling length is longer enough to guarantee a pretty low inter-ring crosstalk. When Λ is 25 μm and wavelength is 1550 nm, the maximum L_c has an order of 10^{10} m for the HE_{11} mode and the minimum L_c has an order of 10^7 m for EH_{41} related OAM mode.

When the propagation length is 100 km, Figure 3 shows the inter-ring crosstalk of HE_{11} mode (best case) and EH_{41} related OAM mode (worst case) in adjacent rings as a function of Λ for TA-MOMRF with trench and multi-OAM multi-ring fiber (MOMRF) without trench. Under a ring pitch Λ of 25 μm , the crosstalk in adjacent rings of TA-MOMRF with trench is -99.3 dB for HE_{11} mode and -45.6 dB for EH_{41} related OAM mode, while -68.9 dB for HE_{11} mode and -0.7 dB for EH_{41} related OAM mode in MOMRF without trench. For MOMRF without trench, the ring pitch should be as large as 32 μm to achieve a -45 dB crosstalk. Hence, the trench design can greatly reduce the inter-ring crosstalk, especially for high-order OAM modes, which facilitates a compact fiber structure.

To further evaluate the performance of the designed TA-MOMRF, we calculate the inter-ring crosstalk with varied propagation length and wavelength. Figure 4 shows the inter-ring crosstalk of HE_{11} mode and EH_{41} related OAM mode in adjacent rings as a function of propagation length for TA-MOMRF with trench and MOMRF without trench under a ring pitch Λ of 25 μm . The summarized

Table 1 | n_{eff} of fiber eigenmodes in a high-contrast-index ring

Mode	HE_{11}	TE_{01}	HE_{21}	TM_{01}	HE_{31}	EH_{11}
n_{eff}	1.6714	1.67099	1.66966	1.66777	1.66487	1.66424
Mode	HE_{41}	EH_{21}	HE_{51}	EH_{31}	EH_{41}	HE_{61}
n_{eff}	1.65705	1.65666	1.64627	1.6461	1.63275	1.63262

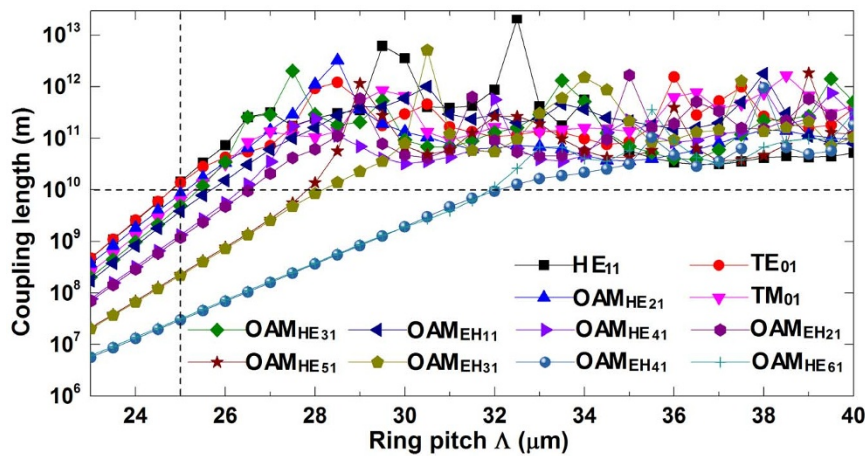


Figure 2 | Coupling length (L_c) of OAM modes in adjacent rings versus ring pitch Δ .

results under propagation lengths of 1 km, 10 km and 100 km are listed in Table 2. One can clearly see from Fig. 4 and Table 2 that the trench structure can effectively reduce the inter-ring crosstalk. Moreover, the pretty low inter-ring crosstalk of TA-MOMRF implies potential use in practical applications, especially for short-distance (e.g. 1 m \sim 1000 m) communications.

Figure 5 shows the inter-ring crosstalk of OAM modes in adjacent rings as a function of wavelength under a propagation length of 100 km. Within a wide wavelength range from 1520 to 1630 nm which covers the whole C band and L band (1530 to 1625 nm), the inter-ring crosstalk in adjacent rings for all 22 modes is less than -26 dB. That is, the designed TA-MOMRF is also compatible with the existing WDM technique. For short-distance (e.g. 1 m \sim 1000 m) communications, similar broadband feature is also achievable with even wider wavelength range and much lower inter-ring crosstalk.

Tolerance to ellipticity and bending. Practical fibers might not be cylindrically symmetric because of the fabrication defects. The strain, stress, twist and other perturbations can also cause the nonperfect circularity (i.e. ellipticity) of fiber, giving rise to birefringence and polarization mode dispersion. Additionally, fiber bending can also induce birefringence. Considering that OAM modes are composed of fiber eigenmodes, i.e. the combination of even and odd modes of HE_{m1} or EH_{n1} with a $\pm\pi/2$ phase shift, the ellipticity of ring and fiber bending can affect the mode profile and purity of OAM modes, resulting in the mode coupling and crosstalk.

We study the impacts of the ellipticity of ring and fiber bend radius on the performance of OAM modes. Figure 6(a) shows the n_{eff}

difference between even and odd fiber eigenmodes as a function of the ellipticity of ring. One can clearly see that high-order OAM modes (EH_{31} , HE_{41} , EH_{41} , HE_{51} and HE_{61} related OAM modes) feature stronger tolerance to the ellipticity variations compared to low-order modes (HE_{11} mode, EH_{11} , HE_{21} , EH_{21} and HE_{31} related OAM modes). For low-order modes, the n_{eff} difference between even and odd fiber eigenmodes increases with the ellipticity of ring. When the ellipticity is 2%, the maximum n_{eff} difference is 1.76×10^{-4} for the EH_{11} related OAM modes. For high-order OAM modes, the calculated n_{eff} difference between the even and odd fiber eigenmodes is around 1×10^{-9} . The high-order OAM modes show enhanced tolerance to the ellipticity variations, which can be explained with the fact that high-order OAM modes have more azimuthal periods in their transverse field distribution, resulting in the mitigation of asymmetric effects from ellipticity. Figure 6(b) shows n_{eff} difference between even and odd fiber eigenmodes as a function of the fiber bend radius. When reducing the bend radius from 100 to 1 cm, high-order OAM modes having more azimuthal periods in their transverse field distribution feature stronger tolerance to the fiber bending effect, while the n_{eff} difference between even and odd fiber eigenmodes of low-order modes increases. The maximum n_{eff} difference is 1.84×10^{-4} for the EH_{11} related OAM modes under a fiber bend radius of 1 cm.

The ellipticity of ring and fiber bending cause n_{eff} difference between even and odd fiber eigenmodes that form OAM modes. Such n_{eff} difference gives rise to temporal walk-off effect upon propagation. Two parameters named 2π walk-off length ($L_{2\pi}$) and 10-ps walk-off length ($L_{10 \text{ ps}}$) are adopted to characterize the intra-mode

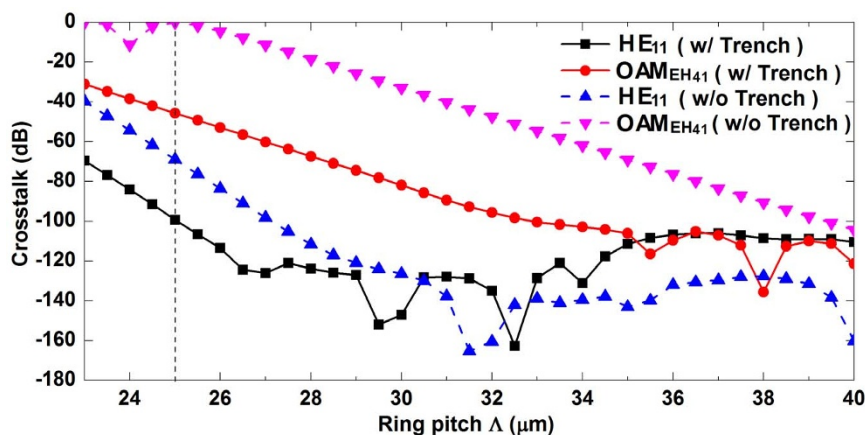


Figure 3 | Inter-ring crosstalk of HE_{11} mode and EH_{41} related OAM mode in adjacent rings with and without trench versus ring pitch Δ under a propagation length of 100 km.

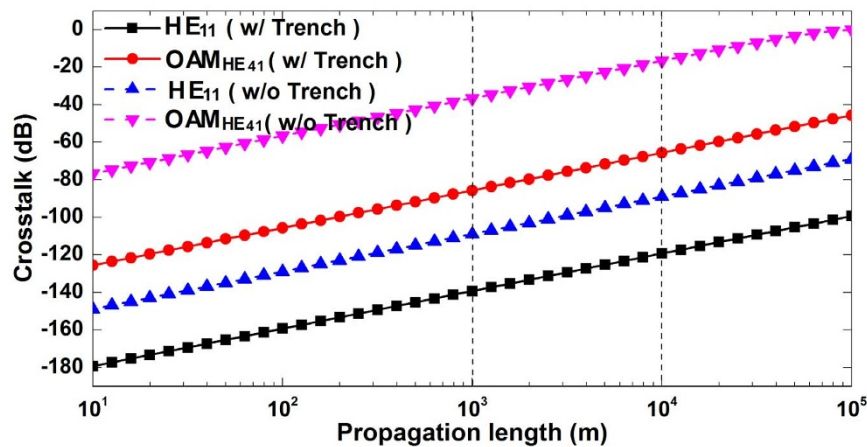


Figure 4 | Inter-ring crosstalk of HE_{11} mode and EH_{41} related OAM mode in adjacent rings with and without trench versus propagation length.

walk-off effect of OAM modes²². Figure 7(a) and (b) plot 2π walk-off length and 10-ps walk-off length for different OAM modes as functions of ellipticity and bend radius, respectively. It can be clearly seen that high-order OAM modes with more azimuthal periods in their transverse field distribution feature longer 2π walk-off length and 10-ps walk-off length. For low-order OAM modes, both 2π walk-off length and 10-ps walk-off length decrease as increasing the ellipticity or reducing the bend radius.

The n_{eff} difference between even and odd fiber eigenmodes due to ellipticity of ring and fiber bending can affect the profile and purity of OAM mode and cause OAM mode coupling and crosstalk. OAM channels with low crosstalk are highly desired for optical communications using OAM multiplexing⁵. In order to assess the crosstalk among different OAM modes, we study the OAM spectra which are also known as the charge weight distribution of OAM modes defined by the electric field overlap integral of the achieved modes and the corresponding pure eigenmodes of an ideal ring fiber²³.

Figure 8(a) and (b) show two examples of calculated OAM spectra for the HE_{21} and HE_{61} related OAM modes under an ellipticity of 0.5%. One can clearly see that the HE_{21} and HE_{61} related OAM modes introduce low-level crosstalk less than -32 and -22 dB respectively to all other 21 modes (17 OAM ones).

Figure 9(a)–(f) show another two examples of calculated OAM spectra for the HE_{21} and HE_{61} related OAM modes under different fiber bend radii of 5, 2 and 1 cm. It can be clearly seen that the HE_{21} and HE_{61} related OAM modes contribute low-level crosstalk less than -28 and -40 dB respectively to all other 21 modes (17 OAM ones) under a fiber bend radius of 5 cm. For a fiber bend radius of 2 cm, low-level crosstalk less than -20 and -40 dB from HE_{21} and HE_{61} related OAM modes are induced to all other 21 modes (17 OAM ones). When further reducing the fiber bend radius to 1 cm, the maximum crosstalk from HE_{21} and HE_{61} related OAM modes increases to -14.9 and -37.3 dB, respectively.

The designed fiber features favorable tolerance to both small ellipticity of ring and small fiber bending. With the increase of ellipticity or the decrease of bend radius, the mode crosstalk also increases. In the case of relatively large mode crosstalk, multiple-input multiple-output (MIMO) technique^{24,25} and low-density parity-check

(LDPC) coding²⁶ might be employed to enable mitigation of crosstalk effects and improve the transmission performance.

Discussion

Benefiting from the high-contrast-index ring structure and trench design, the proposed TA-MOMRF offers simultaneous low-level inter-mode crosstalk and inter-ring crosstalk within a wide wavelength range (1520 to 1630 nm). For optical communications, it is possible to transmit 57266 channels in total ($19 \text{ rings} \times 22 \text{ modes} \times 137 \text{ wavelengths}$ from 1520 to 1630 nm with 100-GHz spacing) with negligible inter-channel crosstalk in a single TA-MOMRF, which could increase 57266 times total transmission capacity and 418 times aggregate spectral efficiency compared with a single channel transmission. For example, when using 42.8-Gbaud/s 16-ary quadrature amplitude modulation (16-QAM) signal for each channel⁵, one might achieve 9.8-Pbit/s total transmission capacity and 1337.6-bit/s/Hz aggregate spectral efficiency.

The designed TA-MOMRF, fully exploring the spatial domain and limited space resources, is not a simple combination of two concepts of single-ring OAM fiber and multi-core fiber which would not be able to simultaneously support multiple OAM modes (22 modes) in multiple rings (19 rings) in a compact fiber design (130 μm cladding diameter) with both low-level inter-mode crosstalk and inter-ring crosstalk over 110 nm wavelength range. These distinct features come from the optimized design of the geometric parameters of ring structure and trench structure, which also offers favorable tolerance to both small ellipticity of ring (< -22 dB crosstalk under an ellipticity of 0.5%) and small bend radius (< -20 dB crosstalk under a bend radius of 2 cm) of practical fibers.

The calculated results shown in Fig. 4 and Table 2 indicate that the inter-ring crosstalk is lower than -45 dB for all 22 modes in adjacent rings even under a 100-km propagation length. However, propagation loss is not considered here. For long-distance transmission, one of the most important limiting effects would be the loss. Fiber structure using high-doping materials might induce relatively large loss. The recent ring fiber OAM transmission showed a propagation loss of ~ 1.6 dB/km^{7,27}, which is larger than the loss of typical single-mode fiber (< 0.2 dB/km). The large loss of OAM ring fiber might be due to the high doping of the ring. The designed TA-MOMRF might show relatively larger loss because of the use of even higher-doping material. Actually, there is a trade-off between the tight light confinement or inter-mode crosstalk and the loss. High-contrast-index ring fiber design benefits tight mode confinement and increased effective refractive index difference among different OAM modes and resultant low-level inter-mode crosstalk, while the loss of the ring fiber is relatively large.

Table 2 | Crosstalk corresponding to Fig. 4 at 1, 10, 100 km

	HE_{11} w/Trench	HE_{11} w/o Trench	$OAM_{EH_{41}}$ w/Trench	$OAM_{EH_{41}}$ w/o Trench
1 km	-139.3 dB	-108.9 dB	-85.6 dB	-36.6 dB
10 km	-119.3 dB	-88.9 dB	-65.6 dB	-16.6 dB
100 km	-99.3 dB	-68.9 dB	-45.6 dB	-0.7 dB

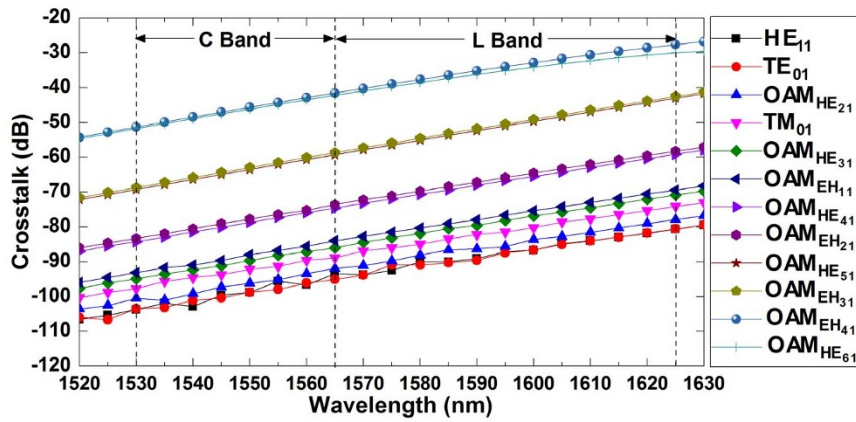


Figure 5 | Crosstalk of OAM modes in adjacent rings versus wavelength under a propagation length of 100 km.

In view of relatively large loss, the most possible applications using the designed fiber could be short-distance (1 m ~ 1000 m) communications, e.g. broadband optical access network (FTTx) and indoor optical fiber communications to end users²⁸. The combination of multiple OAM modes and multiple rings could offer large transmission capacity by ultrahigh-density SDM with tolerable loss for the short-distance communications. In addition to short-distance communications, the short-length OAM ring fiber might also find interesting applications in nonlinear optical signal processing²⁹.

In order to reduce the loss of the designed fiber, possible solutions might be considered: 1) using low-loss materials while optimizing the geometric structure parameters^{7,27}; 2) using similar photonic crystal

fiber structure to confine light in the air gap region to reduce the loss³⁰.

Methods

Mode analyses. We use 2D finite element analysis in the COMSOL software package to compute the effective refractive index (n_{eff}) of fiber eigenmodes as well as the electric field and phase distributions of OAM modes. A circular perfectly matched layer (PML) is used to absorb the incident electromagnetic waves at the outer boundary of cladding. In the ring core domain, the maximum size of grid is set to be 100 nm to ensure the precision of simulation.

Coupling coefficient. In order to analyze the coupling behavior and resultant interring crosstalk in the designed fiber, the coupling coefficient C_{pq} between two adjacent rings (p, q) in a fiber, which determines the coupling length $L_c = \pi/(2\kappa)$, can be calculated using the similar coupled mode theories by Marcuse and Snyder^{31,32}.

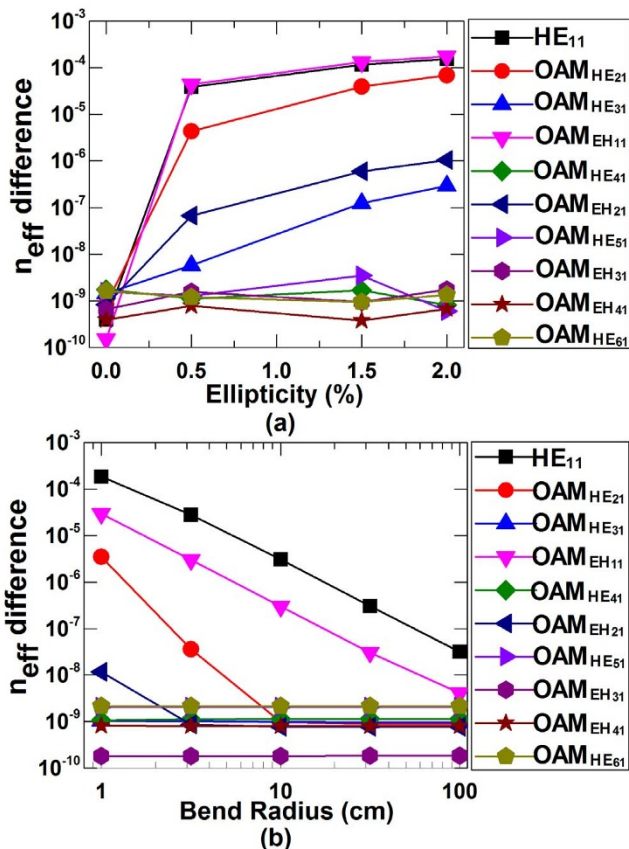


Figure 6 | Effective refractive index (n_{eff}) difference between even and odd fiber eigenmodes as functions of (a) ellipticity of ring and (b) fiber bend radius.

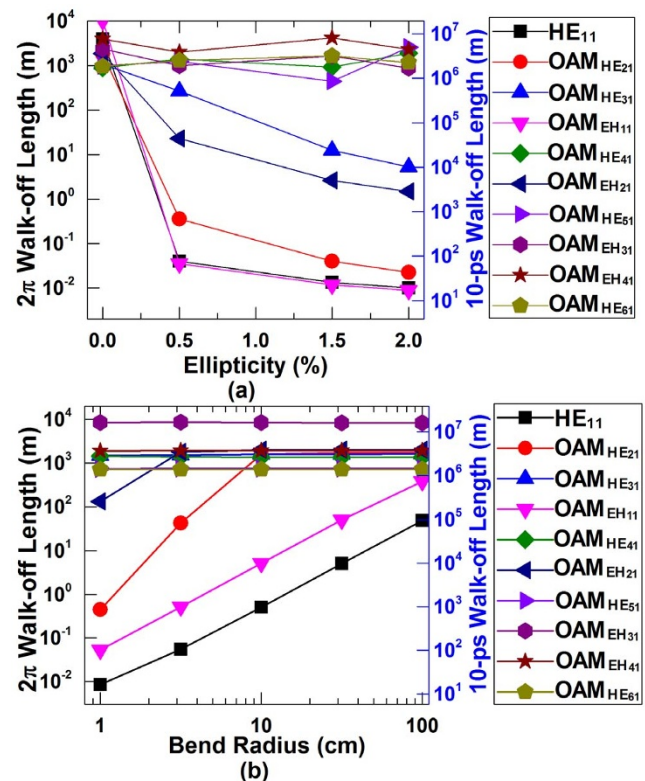


Figure 7 | 2π walk-off length and 10-ps walk-off length for different OAM modes as functions of (a) ellipticity of ring and (b) fiber bend radius.

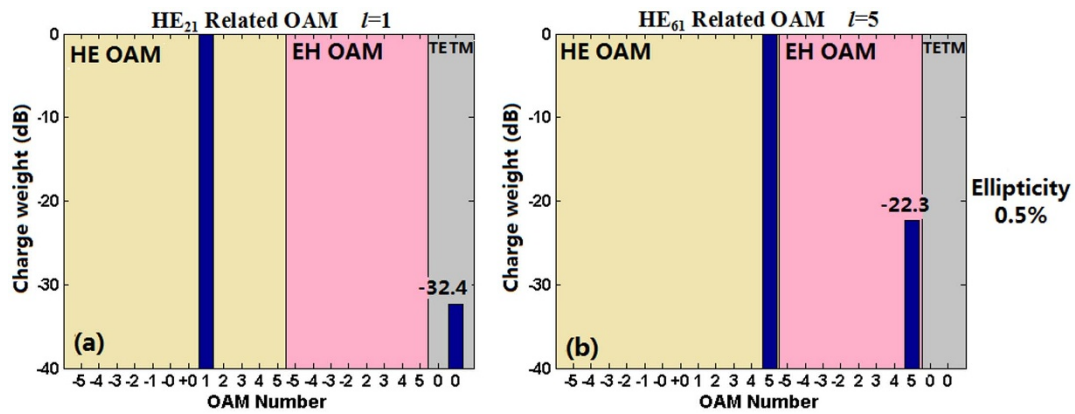


Figure 8 | OAM spectra for (a) HE₂₁ and (b) HE₆₁ related OAM modes under an ellipticity of 0.5%. The OAM numbers “-0” and “+0” denote modes $HE_{11}^{even} \pm i \times HE_{11}^{odd}$.

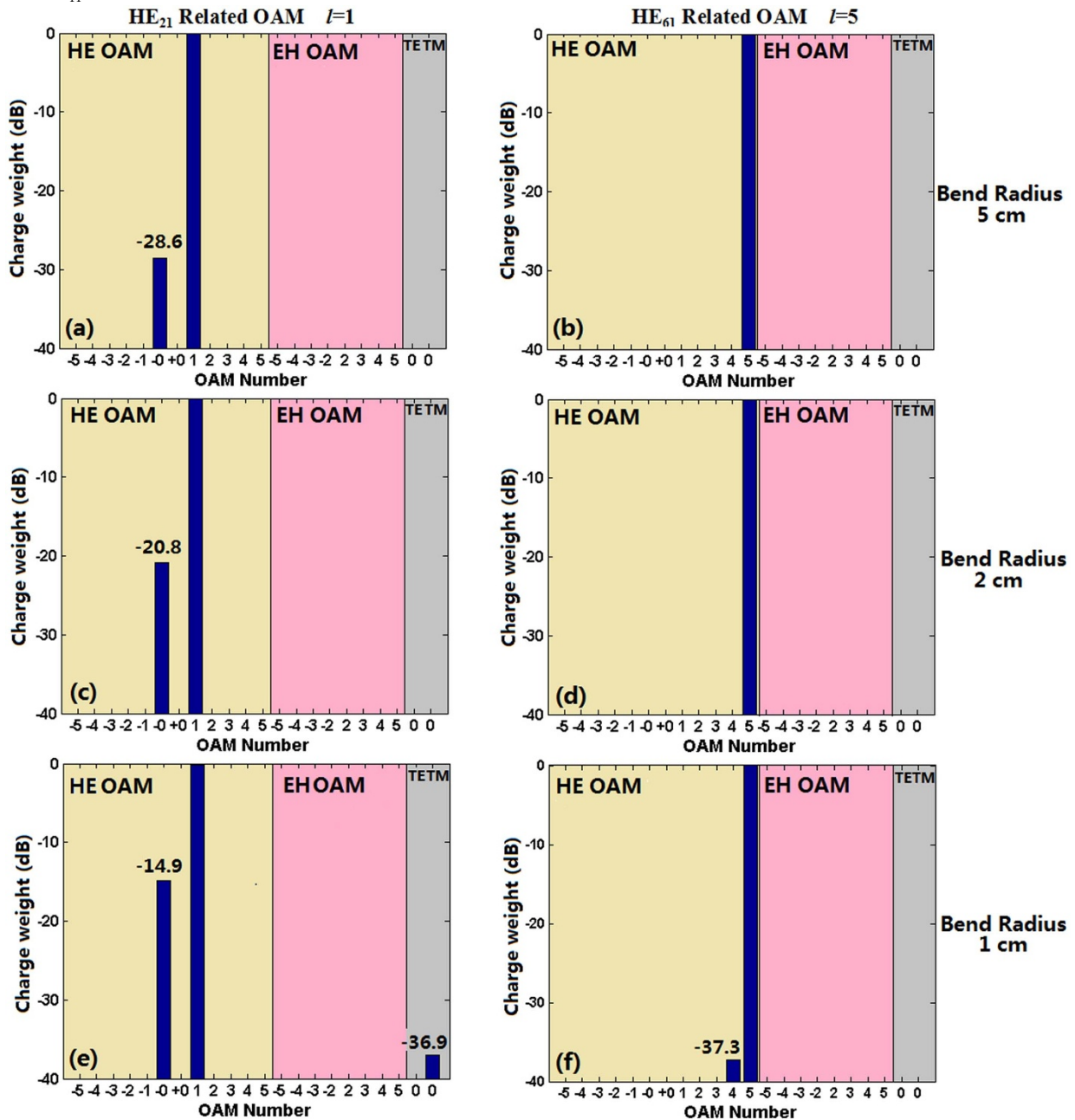


Figure 9 | OAM spectra for (a)(c)(e) HE₂₁ and (b)(d)(f) HE₆₁ related OAM modes under different fiber bend radii of (a)(b) 5 cm, (c)(d) 2 cm and (e)(f) 1 cm. The OAM numbers “-0” and “+0” denote modes $HE_{11}^{even} \pm i \times HE_{11}^{odd}$.



$$C_{pq} = \frac{k}{4(N_p N_q)^{1/2}} \left(\frac{\epsilon_0}{\mu_0} \right)^{1/2} \iint_{\infty} (n^2(x, y) - \bar{n}^2(x, y)) \cdot \vec{e}_p^*(x, y) \cdot \vec{e}_q(x, y) dx dy \quad (1)$$

where $N_p = \frac{1}{2} \iint_{\infty} \vec{e}_p(x, y) \times \vec{h}_p^*(x, y) \cdot \vec{u}_z dx dy$ and $N_q = \frac{1}{2} \iint_{\infty} \vec{e}_q(x, y) \times \vec{h}_q^*(x, y) \cdot \vec{u}_z dx dy$ are

normalization terms. $\vec{e}_p(x, y)$ ($\vec{h}_p(x, y)$) and $\vec{e}_q(x, y)$ ($\vec{h}_q(x, y)$) represent the transverse electric (magnetic) fields of the guided modes of each independent single-ring fiber. k is the wave number in vacuum. ϵ_0 and μ_0 denote the permittivity and permeability of vacuum, respectively. \vec{u}_z is the unit vector along the z -axis direction. $n(x, y)$ and $\bar{n}(x, y)$ are the refractive index profiles of the two-ring fiber and the single-ring fiber, respectively. Note that the integral of Eq. (1) has actually only to be calculated over the region where $\Delta n^2(x, y) = n^2(x, y) - \bar{n}^2(x, y) \neq 0$, i.e. non-null only in the one of two rings.

Considering two identical rings with a spacing of d , we have approximate expressions of $\vec{e}_q(x, y) = \vec{e}_p(x - d, y)$ and $N_p = N_q$. Consequently, Eq. (1) can be simplified and written by²¹

$$C_{pq} = \frac{k}{4N_p} \left(\frac{\epsilon_0}{\mu_0} \right)^{1/2} \iint_{\infty} (n^2(x, y) - \bar{n}^2(x, y)) \cdot \vec{e}_p^*(x, y) \cdot \vec{e}_p(x - d, y) dx dy \quad (2)$$

Therefore, two field calculations ($\vec{e}_p(x, y)$, $\vec{e}_q(x, y)$) are required when using Eq. (1) while only one field calculation ($\vec{e}_p(x, y)$) is needed by applying Eq. (2). Similar computing precisions are provided by Eq. (1) and Eq. (2) giving reliable results for the coupling coefficients.

Walk-off length. The n_{eff} difference between even and odd fiber eigenmodes that compose OAM modes leads to temporal walk-off effects upon propagation.

2π walk-off length ($L_{2\pi}$) represents the propagation length when the even and odd fiber eigenmodes walk off to each other with a relative phase shift of 2π , which is written by²²

$$L_{2\pi} = \frac{\lambda}{n_{\text{eff}}^{\text{even}} - n_{\text{eff}}^{\text{odd}}} \quad (3)$$

where λ is the wavelength in vacuum. $n_{\text{eff}}^{\text{even}}$ and $n_{\text{eff}}^{\text{odd}}$ are effective refractive index of even and odd fiber eigenmodes, respectively.

The walk-off effect between the even and odd fiber eigenmodes distorts the profile of the OAM mode and resultant mode purity, resulting in the mode coupling and crosstalk. It is noted that such behavior features periodic and the period is equal to $L_{2\pi}$.

10-ps walk-off length ($L_{10 \text{ ps}}$) denotes the propagation length when the even and odd fiber eigenmodes have a 10-ps temporal walk off, which is expressed by²²

$$L_{10 \text{ ps}} = \frac{c \times \Delta t}{n_{\text{eff}}^{\text{even}} - n_{\text{eff}}^{\text{odd}}} \quad (4)$$

where c is the light velocity in vacuum and $\Delta t = 10 \text{ ps}$ is the temporal walk off time.

$L_{10 \text{ ps}}$ characterizes the impact of temporal walk-off on the signal quality. For 10-Gbaud/s signals, 10-ps temporal walk-off corresponds to one-tens of the symbol period. Consequently, tolerable signal qualities of 10-Gbaud/s signals are achievable after the $L_{10 \text{ ps}}$ propagation.

OAM spectra. OAM spectra, also known as OAM charge weight distributions, are written by²³

$$C_i = \frac{\iint_{\infty} e(x, y) \cdot \psi_i^*(x, y) dx dy}{\left(\iint_{\infty} e(x, y) \cdot e^*(x, y) \iint_{\infty} \psi_i(x, y) \cdot \psi_i^*(x, y) \right)^{1/2}} \quad (5)$$

where $|C_i|^2$ is the OAM charge weight and $\sum |C_i|^2 = 1$. $e(x, y)$ is the electric field of the achieved mode in a perturbed fiber (e.g. in presence of ellipticity of ring or fiber bending). $\psi_i(x, y)$ is the electric field of eigenmodes in an ideal ring fiber.

Eq. (5) can be used to estimate the mode coupling and crosstalk in presence of perturbations such as the ellipticity of ring and fiber bending.

- Allen, L., Beijersbergen, M. W., Spreeuw, R. J. C. & Woerdman, J. P. Orbital angular momentum of light and the transformation of Laguerre-Gaussian laser modes. *Phys. Rev. A* **45**, 8185–8189 (1992).
- Furhapter, S., Jesacher, A., Bernet, S. & Ritsch-Marte, M. Spiral phase contrast imaging in microscopy. *Opt. Express* **13**, 689–694 (2005).
- Grier, D. A revolution in optical manipulation. *Nature* **424**, 810–816 (2003).
- Mair, A., Vaziri, A., Weihs, G. & Zeilinger, A. Entanglement of the orbital angular momentum states of photons. *Nature* **412**, 313–316 (2001).
- Wang, J. *et al.* Terabit free-space data transmission employing orbital angular momentum multiplexing. *Nature Photon.* **6**, 488–496 (2012).
- Tamburini, F. *et al.* Encoding many channels on the same frequency through radio vorticity: first experimental test. *New J. Phys.* **14**, 033001 (2012).

- Bozinovic, N. *et al.* Terabit-scale orbital angular momentum mode division multiplexing in fibers. *Science* **340**, 14545–1548 (2013).
- Ramachandran, S., Bozinovic, N., Gregg, P., Golowich, S. E. & Kristensen, P. Optical vortices in fibres: a new degree of freedom for mode multiplexing, in *Proceedings of the European Conference and Exhibition on Optical Communication* paper Tu.3.F.3, Amsterdam Netherlands (Optical Society of America, 2012).
- Yan, Y. *et al.* Fiber coupler for generating orbital angular momentum modes. *Opt. Lett.* **36**, 4269–4271 (2011).
- Yan, Y. *et al.* Fiber structure to convert a Gaussian beam to higher-order optical orbital angular momentum modes. *Opt. Lett.* **37**, 3294–3296 (2012).
- Salsi, M. *et al.* Mode-division multiplexing of 2 100 Gb/s channels using an LCOS-based spatial modulator. *J. Lightwave Technol.* **30**, 618–623 (2012).
- Tu, J., Saitoh, K., Koshiba, M., Takenaga, K. & Matsuo, S. Design and analysis of large-effective-area heterogeneous trench-assisted multi-core fiber. *Opt. Express* **20**, 15157–15170 (2012).
- Xia, C. *et al.* Hole-assisted few-mode multi-core fiber for high density space-division multiplexing, in *Proceedings of the Photonics Society Summer Topical Meeting Series, 2012 IEEE paper TuC4.2*, Seattle, WA (IEEE Photonics Society, 2012).
- Li, S. H. & Wang, J. A multi-ring multi-OAM-mode fiber for high-density space-division multiplexing (7 rings \times 22 OAM modes), in *Proceedings of Photonics Conference (IPC)*, 2013 IEEE paper TuG2.3, Bellevue Washington (IEEE Photonics Society, 2013).
- Li, S. H. & Wang, J. Multi-orbital-angular-momentum multi-ring fiber for high-density space-division multiplexing. *IEEE Photon. J.* **5**, 7101007 (2013).
- Sakaguchi, J. *et al.* 305 Tb/s space division multiplexed transmission using homogeneous 19-core fiber. *J. Lightwave Technol.* **31**, 554–562 (2013).
- Feng, X. *et al.* Dispersion-shifted all-solid high index-contrast microstructured optical fiber for nonlinear applications at 1.55 μm . *Opt. Express* **17**, 20249–20255 (2009).
- Poletti, F. *et al.* All-solid highly nonlinear singlemode fibers with a tailored dispersion profile. *Opt. Express* **19**, 66–80 (2011).
- Dashti, P. Z., Alhassen, F. & Lee, H. P. Observation of orbital angular momentum transfer between acoustic and optical vortices in optical fiber. *Phys. Rev. Lett.* **96**, 043604 (2006).
- Koshiba, M., Saitoh, K. & Kokubun, Y. Heterogeneous multi-core fibers: proposal and design principle. *IEICE Electron. Express* **6**, 98–103 (2009).
- Mothe, N. & Bin, P. D. Numerical analysis of directional coupling in dual-core microstructured optical fibers. *Opt. Express* **17**, 15778–15789 (2009).
- Yue, Y. *et al.* Mode properties and propagation effects of optical orbital angular momentum (OAM) modes in a ring fiber. *IEEE Photon. J.* **4**, 535–543 (2012).
- Molina-Terriza, G., Torres, J. P. & Torner, L. Management of the angular momentum of light: Preparation of photons in multidimensional vector states of angular momentum. *Phys. Rev. Lett.* **88**, 013601 (2002).
- Randel, S. *et al.* 6×56 -Gb/s mode-division multiplexed transmission over 33-km few-mode fiber enabled by 6×6 MIMO equalization. *Opt. Express* **19**, 16697–16707 (2011).
- Huang, H. *et al.* 4×4 MIMO equalization to mitigate crosstalk degradation in a four-channel free-space orbital-angular-momentum-multiplexed system using heterodyne detection, in *Proceedings of the European Conference and Exhibition on Optical Communication* paper Th.1.C.4, London (Optical Society of America, 2013).
- Djordjevic, I. B. & Arabaci, M. LDPC-coded orbital angular momentum (OAM) modulation for free-space optical communication. *Opt. Express* **18**, 24722–24728 (2010).
- Bozinovic, N. *et al.* Orbital angular momentum (OAM) based mode division multiplexing (MDM) over a Km-length fiber in *Proceedings of the European Conference and Exhibition on Optical Communication* paper Th.3.C.6, Amsterdam Netherlands (Optical Society of America, 2012).
- Djordjevic, I. B. Heterogeneous transparent optical networking based on coded OAM modulation. *IEEE Photon. J.* **3**, 531–537 (2011).
- Yue, Y. *et al.* Octave-spanning supercontinuum generation of vortices in an As2S3 ring photonic crystal fiber. *Opt. Lett.* **37**, 1889–1891 (2012).
- Poletti, F. *et al.* Towards high-capacity fibre-optic communications at the speed of light in vacuum. *Nature Photon.* **7**, 279–284 (2013).
- Marcuse, D. Theory of dielectric optical waveguides. Pao, Y. H. & Kelley, P. ed. (Academic Press, New York, 1974).
- Snyder, A. W. & Love, J. D. Optical waveguide theory (Kluwer Academic Publishers, 2000).

Acknowledgments

This work was supported by the National Basic Research Program of China (973 Program) under grant 2014CB340004, the National Natural Science Foundation of China (NSFC) under grants 11274131, 61222502 and L1222026, the Program for New Century Excellent Talents in University (NCET-11-0182), and the Fundamental Research Funds for the Central Universities (HUST) under grants 2012YQ008, 2013ZZGH003, and CXY13Q023. The authors would like to thank Chengcheng Gui, Zhonglai Zhang, Zhidan Xu and Jiaying Zhou for helpful discussions.



Author contributions

J.W. developed the concept and conceived the design. S.H.L. performed the numerical simulations and analyzed the data. J.W. and S.H.L. contributed to writing and finalizing the paper.

Additional information

Competing financial interests: The authors declare no competing financial interests.

How to cite this article: Li, S.H. & Wang, J. A Compact Trench-Assisted Multi-Orbital-Angular-Momentum Multi-Ring Fiber for Ultrahigh-Density Space-Division Multiplexing (19 Rings \times 22 Modes). *Sci. Rep.* 4, 3853; DOI:10.1038/srep03853 (2014).



This work is licensed under a Creative Commons Attribution-NonCommercial-NoDerivs 3.0 Unported license. To view a copy of this license, visit <http://creativecommons.org/licenses/by-nc-nd/3.0>